

ON THE ORIGIN OF THE GLOBAL SCHMIDT LAW OF STAR FORMATION

ANDREY V. KRAVTSOV

Department of Astronomy and Astrophysics and Center for Cosmological Physics,
5640 S. Ellis Ave., The University of Chicago, Chicago IL 60637
e-mail: andrey@oddjob.uchicago.edu
Draft version October 31, 2018

ABSTRACT

One of the most puzzling properties of observed galaxies is the universality of the empirical correlation between the star formation rate and average gas surface density on kiloparsec scales (the Schmidt law). In this study I present results of self-consistent cosmological simulations of high-redshift galaxy formation that reproduce the Schmidt law naturally, without assuming it, and provide some clues to this puzzle. The simulations incorporate the main physical processes critical to various aspects of galaxy formation and have a dynamic range high enough to identify individual star forming regions. The results indicate that the global Schmidt law is a manifestation of the overall density distribution of the interstellar medium (ISM). In particular, the density probability distribution function (PDF) in the simulated disks is similar to that observed in recent state-of-the-art modeling of the turbulent ISM and has a well-defined generic shape. The shape of the PDF in a given region of the disk depends on the local average surface density Σ_g . The dependence is such that the fraction of gas mass in the high-density tail of the distribution scales as Σ_g^{n-1} with $n \approx 1.4$, which gives rise to the Schmidt-like correlation. The high-density tail of the PDF is remarkably insensitive to the inclusion of feedback and details of the cooling and heating processes. This indicates that the global star formation rate is determined by the supersonic turbulence driven by gravitational instabilities on large scales, rather than stellar feedback or thermal instabilities on small scales.

Subject headings: cosmology: theory–galaxies: evolution–galaxies: formation–ISM: kinematics and dynamics – ISM: structure – stars: formation–methods: numerical

1. INTRODUCTION

Formation of galaxies is a complicated process involving a variety of physical phenomena on a large range of spatial and temporal scales. Although hierarchical structure formation scenario proved to be a very successful framework for interpreting a wide variety of observational data, much remains to be understood about the processes that shape properties of galaxies. In particular, star formation is one of the most important, yet very poorly understood processes.

On small scales ($\lesssim 10$ – 100 pc), star formation appears to be a complicated and stochastic process. Understanding how stars and stellar clusters form in individual molecular clouds is still sketchy, even in the best studied cases (e.g., Hartmann 2002). It is therefore remarkable that on kiloparsec scales star formation exhibits surprising regularity. Schmidt (1959) first argued that the star formation rate (SFR) in galaxies is a power law function of average gas density. This simple ‘Schmidt’ law

$$\Sigma_{\text{SFR}} \propto \Sigma_g^n, \quad (1)$$

where Σ_{SFR} and Σ_g are the surface densities of young stars and gas averaged on a large (\sim kpc) scale, was found to hold for a wide range of galaxy types, star formation rates, and gas densities (Kennicutt 1983, 1989, 1998a,b). The star formation histories of the Local Group dwarfs indicate that the Schmidt law applied at high redshifts (Gnedin 2000). The power-law index of the correlation falls in the range $n \approx 1.3$ – 1.6 , depending on the tracers used and the scales considered (Kennicutt 1998a). In addition, star formation rate in galaxies declines sharply below a critical threshold surface density of ~ 5 – $10 M_\odot \text{pc}^{-2}$ (e.g., Kennicutt 1989; Martin & Kennicutt 2001, and references therein). This density is thought to be associated with large-scale gravitational and shearing stability thresholds, although details of the mechanism are still uncertain. Nevertheless, at high gas densities the form of the Schmidt law appears to be remarkably consistent from galaxy to galaxy, both in terms of slope and absolute efficiency (i.e., normalization of the relation).

Despite the apparent simplicity, a unique explanation for the Schmidt law proved to be elusive. To a large extent, the prob-

lem is that the Schmidt law can be explained by any process in which gas consumption time depends on the local average dynamical time ($\propto \rho^{-1/2}$). A wide variety of possible models with such scaling have been proposed in the last three decades (see Elmegreen 2002, for a review). Nevertheless, the universality of the star formation efficiency and the slope of the Schmidt law in the face of complexity of star formation on small scales remains a puzzle. In this *Letter* I present results of self-consistent cosmological simulations of high-redshift galaxy formation that reproduce the Schmidt law naturally, without assuming it, and provide some clues to this puzzle.

2. IMPLEMENTATION OF STAR FORMATION

The simulations presented in this paper were performed using the Eulerian gasdynamics+ N -body Adaptive Refinement Tree (ART) code. The code is based on the cell-based approach to adaptive mesh refinement (AMR) developed by Khokhlov (1998). The algorithm uses a combination of multi-level particle-mesh (Kravtsov et al. 1997; Kravtsov 1999) and shock-capturing Eulerian methods (van Leer 1979; Colella & Glaz 1985) to follow the evolution of the DM and gas, respectively. High dynamic range is achieved by applying adaptive mesh refinement to both gasdynamics and gravity calculations.

Several physical processes critical to various aspects of galaxy formation are implemented in the code: star formation, metal enrichment and thermal feedback due to the supernovae type II and type Ia (SNII/Ia), self-consistent advection of metals, metallicity- and density-dependent cooling and UV heating due to cosmological ionizing background using cooling and heating rates tabulated for the temperature range $10^2 < T < 10^9$ K and a grid of densities, metallicities, and UV intensities using the Cloudy code (ver. 96b4, Ferland et al. 1998). The cooling and heating rates take into account Compton heating/cooling of plasma, UV heating, atomic and molecular cooling. The detailed implementation of these processes will be described elsewhere (Kravtsov 2003). As I will show below, the results presented in this paper are not sensitive to the details of these processes. Here I will focus on the implementation of star for-

mation, the process which is the subject of this study.

In numerical simulations star formation is usually assumed to occur in certain “star forming” regions identified using some specific criteria. The gas in such regions is then converted into stars on a characteristic gas consumption time scale, τ_* : $\dot{\rho}_* = \rho_g / \tau_*$. Observationally, the efficiency of star formation on small ($\lesssim 100$ pc) scales in the densest regions of the ISM is significantly higher than the low global efficiency indicated by the Schmidt law (e.g., Elmegreen 2002). This means that the value of τ_* and, perhaps more importantly, its density dependence in simulations should be different depending on whether star forming regions are resolved. Clearly, the use of the Schmidt law is observationally motivated only on scales $\gtrsim 1$ kpc. Although implementations vary, galaxy formation simulations usually adopt gas consumption time that scales as $\tau_* \propto \max(t_{\text{cool}}, t_{\text{dyn}})$, where t_{cool} and t_{dyn} are the local cooling and dynamical time, respectively. In even moderately dense regions, $t_{\text{cool}} \ll t_{\text{dyn}}$ and $\tau_* \propto t_{\text{dyn}} \propto \rho^{-1/2}$, which results in the Schmidt-like star formation law: $\dot{\rho}_* \propto \rho_g^{1.5}$.

In this study, a “minimal” star formation prescription was used. Namely, the stars were formed with a *constant* τ_* so that $\dot{\rho}_* \propto \rho_g$. This “constant efficiency” model on the scale of star forming regions is well motivated by observations (e.g., Young et al. 1996; Wong & Blitz 2002). The star formation was allowed to take place only in the coldest and densest regions, $T < T_{\text{SF}}$ and $\rho_g > \rho_{\text{SF}}$, but no other criteria (like the collapse condition $\nabla \cdot \mathbf{v} < 0$) were imposed. I used $\tau_* = 4$ Gyrs, $T_{\text{SF}} = 9000$ K, and $\rho_{\text{SF}} = 1.64 M_\odot \text{pc}^{-3}$ or atomic hydrogen number density of $n_{\text{H}} = 50 \text{cm}^{-3}$. The adopted values of T_{SF} and ρ_{SF} are quite different from the typical temperatures and density of star forming molecular cores: $T \lesssim 30 - 50$ K and $n_{\text{H}} \gtrsim 10^4 \text{cm}^{-3}$. They are, however, more appropriate to identify star forming regions on ~ 100 pc scales which are resolved in the presented simulations. In practice, T_{SF} is not relevant because most of the gas at $\rho > \rho_{\text{SF}}$ is at temperatures of just a few hundred degrees Kelvin. The adopted gas consumption time scale τ_* is derived from the observed normalization of the Schmidt law.

Algorithmically, star formation events are assumed to occur once every global time step $\Delta t_0 \lesssim 10^7$ yrs, the value close to the observed time scales (e.g., Hartmann 2002). Collisionless stellar particles with mass $m_* = \dot{\rho}_* \Delta t_0$ are formed in every unsplit mesh cell during star formation events. The mass of stellar particles is restricted to be larger than $10^4 M_\odot$ but smaller than $2/3$ of the gas mass contained in the parent cell. This is done in order to keep the number of stellar particles computationally tractable while avoiding a sudden dramatic decrease in the local gas density.

Once formed, each stellar particle is treated as a single-age stellar population and its feedback on the surrounding gas is implemented accordingly. I use the word feedback in a broad sense to include injection of energy and heavy elements (metals) via stellar winds and supernovae and secular mass loss. Specifically, in the simulations analyzed here, I assumed that the stellar initial mass function (IMF) is described by the Miller & Scalo (1979) functional form with stellar masses in the range $0.1 - 100 M_\odot$. All stars with $M_* > 8 M_\odot$ deposit 2×10^{51} ergs of thermal energy and a mass $f_Z M_*$ of heavy elements in their parent cell (no delay of cooling was introduced in these cells). The metal fraction is $f_Z = \min(0.2, 0.01 M_* - 0.06)$, which crudely approximates the results of Woosley & Weaver (1995). In addition, the stellar particles return a fraction of their mass and metals to the surrounding gas at a secular rate $\dot{m}_{\text{loss}} = m_* C_0 (t -$

$t_{\text{birth}} + T_0)^{-1}$ with $C_0 = 0.05$ and $T_0 = 5$ Myr (Jungwiert et al. 2001). The code also accounts for SNIa feedback assuming a rate that slowly increases with time and broadly peaks at the population age of 1 Gyr. I assume that a fraction of 5×10^{-3} of mass in stars between 3 and $8 M_\odot$ explodes as SNIa over the entire population history and each SNIa dumps 2×10^{51} ergs of thermal energy and ejects $1.3 M_\odot$ of metals into parent cell. For the assumed IMF, 75 SNII (instantly) and 11 SNIa (over several billion years) are produced by a $10^4 M_\odot$ stellar particle.

3. NUMERICAL SIMULATIONS

In this paper I present two simulations of the early ($z \geq 4$) stages of evolution for a galaxy of typical mass: $\approx 10^{12} h^{-1} M_\odot$ at $z = 0$. At the analyzed epochs, the galaxy has already built up a significant portion of its final mass: $1.3 \times 10^{10} h^{-1} M_\odot$ at $z = 9$ and $2 \times 10^{11} h^{-1} M_\odot$ at $z = 4$. The evolution is started from a random realization of a gaussian density field at $z = 50$ in a periodic box of $6h^{-1}$ Mpc with an appropriate power spectrum and is followed assuming flat Λ CDM model: $\Omega_0 = 1 - \Omega_\Lambda = 0.3$, $\Omega_b = 0.043$, $h = H_0/100 = 0.7$, $n_s = 1$, and $\sigma_8 = 0.9$. The parameters have their usual meaning and are consistent with recent cosmological constraints.

To increase the mass resolution, a low-resolution simulation was run first and a galactic-mass halo was selected. A lagrangian region corresponding to five virial radii of the object at $z = 0$ was then identified at $z = 50$ and re-sampled with additional small-scale waves (Klypin et al. 2001). The total number of DM particles in the high-resolution lagrangian region is 2.64×10^6 and their mass is $m_{\text{DM}} = 9.18 \times 10^5 h^{-1} M_\odot$. Outside the high-resolution region the matter distribution was sampled with $\approx 3 \times 10^5$ higher mass particles.

As the matter distribution evolves, the code adaptively and recursively refines the mesh in high-density regions. In the simulations I present, two main refinement criteria were used: gas and DM mass in each cell. The code used a uniform 64^3 grid to cover the entire computational box. The lagrangian region, however, was always unconditionally refined to the third refinement level, corresponding to the effective grid size of 512^3 . Beyond the third level, a mesh cell was tagged for refinement if its gas *or* DM mass exceeded 0.125 and 0.0625 times the mean mass expected for the average density in each component in the zeroth level (i.e., uniform grid) cell, respectively. The refinement thus follows the collapse of $1.2 \times 10^6 h^{-1} M_\odot$ (gas) and $3.7 \times 10^6 h^{-1} M_\odot$ (DM) mass elements in a quasi-lagrangian fashion.

The maximum allowed refinement level l_{max} was set to nine. A total of $\approx 1.1 \times 10^7$ mesh cells was used at $z = 4$ with $\approx 2.5 \times 10^5$ of them at refinement levels of 8 and 9. The volume of high-density cold star forming disks forming in DM halos was refined to $l_{\text{max}} = 9$. The physical size of mesh cells in the simulations was $\Delta x_l = 26.16 [10/(1+z)] 2^{9-l}$ pc, where l is the cell’s level of refinement. Each refinement level was integrated with its own time step $\Delta t_l = \Delta t_0 2^{-l} \approx 2 \times 10^4 2^{9-l}$ yrs, where $\Delta t_0 \lesssim 10^7$ yrs is the global time step on the zeroth level, set using the CFL condition.

The two analyzed simulations are the same in all respects, except that one included all of the feedback processes described above (energy and metal injection, mass loss, etc.), while the other did not. The simulation with no feedback is designated as NF throughout this paper. Note that the cooling rates in the run with feedback accounted for the local metallicity of the gas, while in the run with no feedback the significantly lower zero-

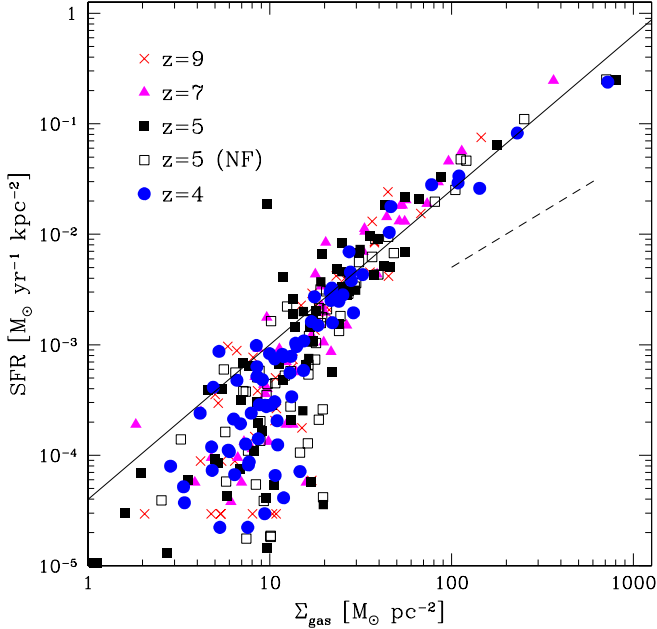


FIG. 1.— Star formation rate surface density vs. gas surface density in the simulated galaxies at different epochs. The open squares show $z = 5$ epoch in the simulation in which no feedback (NF) processes were included. The rates and gas density are averaged over $3.35 [(1+z)/10]$ kpc. The solid line is relation $\text{SFR} \propto \Sigma_{\text{g}}^{1.4}$ while the dashed line is $\text{SFR} \propto \Sigma_{\text{g}}$.

metallicity cooling rates were used.

4. RESULTS

Figure 1 shows the star formation rate per area vs. gas surface density at different epochs in the simulations. Individual points correspond to the level $l = 2$ cells of size $\Delta x_2 = 3.35 [(1+z)/10]$ kpc. Note that the cells represent not a single object but several dozen galaxies with masses $\gtrsim 10^8 h^{-1} M_{\odot}$ distributed in a high resolution ~ 1 Mpc (comoving) lagrangian region. The gas surface density was computed simply as $\Sigma_{\text{gas}} = \rho_{\text{g}} \Delta x_2$ and the SFR in each cell was estimated as $m_* t_*^{-1} \Delta x_2^{-2}$, where m_* is the mass of stars younger than $t_* = 3 \times 10^7$ yrs. The averaging scale and t_* are close to the values typical for observational estimates (see Kennicutt 1998a). The resulting SFR per area and Σ_{gas} are not sensitive to variation in averaging scale and t_* over a large range of values.

The figure shows that the star formation rate is strongly correlated with gas surface density: $\text{SFR} \propto \Sigma_{\text{gas}}^n$ with $n \approx 1.4$ (solid line) for $\Sigma_{\text{gas}} \gtrsim 10 M_{\odot} \text{pc}^{-2}$. At smaller densities the rate rapidly decreases and most $l = 2$ cells with $\Sigma_{\text{gas}} \lesssim 5 M_{\odot} \text{pc}^{-2}$ do not contain young stars (i.e., $\text{SFR} = 0$). The simulations thus reproduce the slope of the empirical Schmidt law and the observed critical threshold for star formation remarkably well. Figure 1 also shows that the relation is universal: it does not depend sensitively on redshift or input physics. The correlation is not sensitive to the variations of averaging scale and t_* by at least a factor of four. This is a non-trivial result because the correlation is observed on kiloparsec scales, while star formation occurs in individual $20 - 50$ pc cells with the *rate simply proportional to the gas density*: $\dot{\rho}_* \propto \rho_{\text{g}}$. The $\text{SFR} \propto \Sigma_{\text{g}}$ correlation is indeed recovered when averaging is done on the scale of individual star forming regions (~ 100 pc). The observed scaling $\text{SFR} \propto \Sigma_{\text{gas}}^{1.4}$ on kpc scales is therefore reproduced naturally when a constant efficiency of star formation is assumed on the scale of molecu-

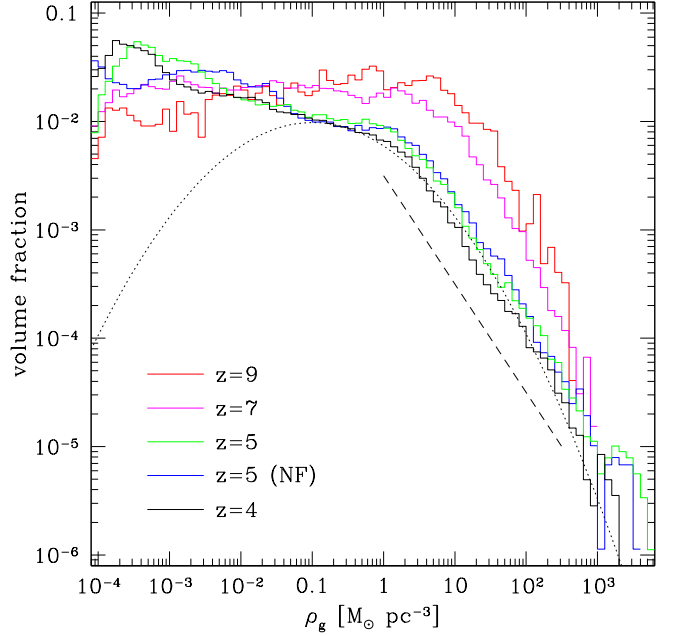


FIG. 2.— Probability distribution function of gas density in the simulated gas disks at different redshifts. The PDF, the fraction of total volume in a given density interval ($\Delta \log_{10} \rho_{\text{g}} = 0.1$), was computed in the regions refined to $l \geq 8$ refinement level. The PDFs are normalized to unity. The histograms show outputs at different epochs; the blue histogram shows results for $z = 5$ output of the run without feedback (NF). The dashed line is $\propto \rho_{\text{g}}^{-1}$, while the dotted line shows a log-normal PDF

lar complexes.

The scatter about the mean of the correlation is rather small ($\sim 0.2 - 0.3$ dex) and is well below the observed scatter. The observed individual rates and densities, however, have errors $\gtrsim 0.2 - 0.3$ dex so larger scatter can be expected. The scatter at any given epoch is even smaller, which is remarkable given that the galaxies at $z \gtrsim 4$ undergo very frequent and violent mergers. The normalization of the correlation is somewhat lower than observed. This can be fixed by lowering τ_* . The gas consumption time is a free parameter of the model and so is the normalization of the $\text{SFR} - \Sigma_{\text{g}}$ correlation.

5. DISCUSSION AND CONCLUSIONS

What mechanism gives rise to the Schmidt law in simulated galaxies and what explains its universality? Some understanding can be gained by considering the density distribution of gas in simulated galaxy disks. Figure 2 shows the probability distribution function (PDF) of gas density in the disks at different epochs. Although the PDF evolves with time, its general shape at every epoch can be characterized by the relatively flat region at $\rho_{\text{g}} \lesssim 1 - 10 M_{\odot} \text{pc}^{-3}$ and a power law distribution at high densities. The high-density tail is also well approximated by the log-normal distribution (dotted line in Fig. 2). The evolution is driven primarily by shocks associated with supersonic turbulence induced by gravitational and shearing instabilities and, occasionally, by tidal interactions during mergers in the gas disks. For instance, the most massive disk in the simulation at $z = 4$ has well-developed large-scale spiral arms and exhibits signs of two minor mergers in progress (Kravtsov 2003).

Stellar feedback appears to have only a minor effect on the overall shape of the PDF. Comparison of PDFs for the feedback and no-feedback (NF) runs at $z = 5$ shows that distribution is remarkably insensitive to the inclusion of several feedback

processes. The only difference is at the lowest gas densities, where the simulation with feedback has considerably more low-density hot gas due to the energy injection by SNe. Note that in terms of morphology of gas distribution the effect of energy injection is significant as the lowest density regions occupy a large fraction of the volume. Globally, the effect of energy feedback on the thermal state of gas in the halos and surrounding intergalactic medium is also significant (Tassis et al. 2002). This makes the insensitivity of the high-density PDF to feedback even more remarkable. The distributions are also not sensitive to the differences in metallicity and cooling rates between feedback and no feedback runs.

The characteristic shape of the PDF in figure 2 has been found in several numerical studies of turbulent ISM. In particular, it is very similar to the density PDF in the 2D disk simulations of Wada & Norman (2001). These authors also found that density PDF is not sensitive to the stellar energy feedback. The log-normal high-density tail of the PDF is thought to be a generic feature of the turbulent (i.e., randomly forced) supersonic flows (e.g., Vázquez-Semadeni 1994; Padoan et al. 1997; Vázquez-Semadeni et al. 2000). The effective pressure in such flows is dominated by turbulent (kinematic) rather than thermal pressure. This may explain the relatively low sensitivity of the density distribution to the details of cooling. The cooling and heating, however, are important in determining the effective equation of state of the gas and thus should definitely also play a role. The gas will become increasingly more compressible as the ratio of the local cooling time to the characteristic crossing time decreases. Higher compressibility would then allow the gas to reach higher densities in converging flows, presumably creating the high-density tail of the distribution and star forming regions. The high-density tail is thus likely to be the result of the driven turbulent cascade in a nearly isothermal gas. Indeed, for the heating/cooling rates adopted in the simulations temperatures of the gas at densities $\rho_g \gtrsim 5 \text{ M}_\odot \text{ pc}^{-3}$ are in the range $\sim 100\text{--}1000 \text{ K}$. The transition to isothermality, however, does not explain the shape of the PDF. The same shape was found in a test simulation in which gas was artificially kept isothermal at $T = 300 \text{ K}$.

The Schmidt law on kiloparsec scales implies that the efficiency of the turbulent build-up of the high-density tail depends on the average gas density at these scales. Clearly, if the PDF shape were independent of average density we would have $\text{SFR} \propto \Sigma_g$. To satisfy the observed non-linear scaling, the fraction of mass in star forming regions should scale as $m_{\text{SF}}/m_g \propto \Sigma_g^{n-1}$, where n is the slope of the Schmidt law, m_g is the total mass of gas in a volume element used in averaging.

Figure 3 shows the density PDFs in 3.35 kpc ($l = 3$) cells with different densities. Although the low-density part of the distribution fluctuates, the largest changes are in the high-density tail which steepens with decreasing gas density. For $\Sigma_g = 18 \text{ M}_\odot \text{ pc}^{-2}$ the maximum density is close to the star formation threshold $\rho_{\text{SF}} = 1.64 \text{ M}_\odot \text{ pc}^{-3}$ adopted in simulations. The inset in the figure 3 shows that the fraction of mass at densities $\rho > \rho_{\text{SF}}$ as a function of average surface density scales as $\propto \Sigma_g^{0.4}$, as expected from the Schmidt law. Interestingly, this can also explain the results of Wong & Blitz (2002) who found that $\text{SFR} \propto \Sigma_{\text{H}_2}^{n_{\text{mol}}}$ with $n_{\text{mol}} \approx 1$ while $\text{SFR} \propto \Sigma_{\text{HI}+\text{H}_2}^n$ with $n \approx 1.4$, where Σ_{H_2} is the density of molecular hydrogen. Most of the gas at pressures $\gtrsim 10^4 \text{ cm}^{-3} \text{ K}$ in their observations is in molecular form. This corresponds to densities of $\gtrsim 1\text{--}5 \text{ M}_\odot \text{ pc}^{-3}$. The molecular gas thus simply traces the high-density tail of the PDF. Figure 3

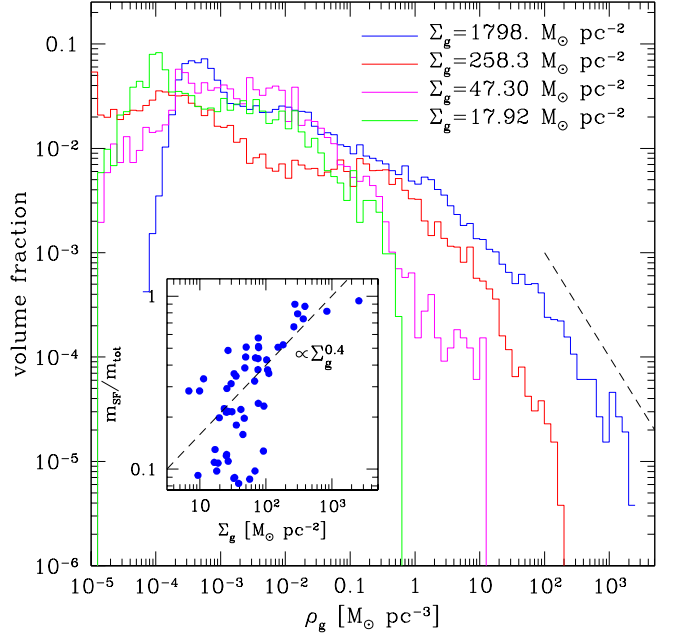


FIG. 3.— Density PDFs in 3.35 kpc ($l = 3$) mesh cells of different surface densities at $z = 4$. The PDFs are normalized to unity. The dashed line is $\propto \rho_g^{-1}$ dependence. The inset plot shows the fraction of mass at densities $\rho > \rho_{\text{SF}}$ as a function of average surface density of cells. The dashed line here shows scaling $\propto \Sigma_g^{0.4}$, expected from the Schmidt law (see text for details).

shows that constant efficiency of the star formation in the densest regions does not contradict the Schmidt law for the total gas density on large scales.

The scatter in m_{SF} for $\Sigma_g \lesssim 10\text{--}20 \text{ M}_\odot \text{ pc}^{-2}$ increases as the maximum density of the PDF fluctuates around ρ_{SF} reflecting the stochastic nature of turbulent flows. The build-up of the high-density tail can be viewed as a random walk of gas elements in density with the probability proportional to the density PDF (Elmegreen 2002). The bottleneck in the rate of gas crossing ρ_{SF} is at low densities at largest scales, which therefore control the mass of gas available for star formation. Indeed, simulations of Wada & Norman (2001) show that the density PDF reaches its “equilibrium” shape on the dynamical time corresponding to the average density of the region.

This scenario can naturally explain the tight connection between the average gas density on kiloparsec scales and star formation on small scales. The universality of the connection can be attributed to the relatively low sensitivity of the density PDF to the details of feedback and precise cooling and heating rates. The efficiency with which driven supersonic turbulence builds up the high-density tail of the PDF depends mainly on the average gas density of the region. Results of this study indicate that the Schmidt law is simply a manifestation of this dependency. It is intriguing that the turbulence may also be responsible for the redistribution of angular momentum and exponential light profiles of galactic disks (e.g., Lin & Pringle 1987; Silk 2001; Slyz et al. 2002).

The modeling of the density dependence and evolution of the PDF is well within the capabilities of the current state-of-the-art numerical simulations of the ISM (e.g., Vázquez-Semadeni et al. 2000; Wada & Norman 2001; Ostriker et al. 2001). This opens the possibility to construct a sound detailed theoretical model of the empirical global star formation law in the very near future.

I would like to thank Anatoly Klypin for many stimulating discussions on star formation. The simulations and analyses presented here were performed on the IBM RS/6000 SP system at the National Energy Research Scientific Computing Center (NERSC) and on the Origin2000 at the National Center for Supercomputing Applications (NCSA). This work was supported by the National Science Foundation under grant No. AST-0206216.

REFERENCES

- Colella, P. & Glaz, H. M. 1985, *J.Comp.Phys.*, 59, 264
 Elmegreen, B. G. 2002, *ApJ*, 577, 206
 Ferland, G. J., Korista, K. T., Verner, D. A., Ferguson, J. W., Kingdon, J. B., & Verner, E. M. 1998, *PASP*, 110, 761
 Gnedin, N. Y. 2000, *ApJ*, 535, L75
 Hartmann, L. 2002, *ApJ*, 578, 914
 Jungwiert, B., Combes, F., & Palouš, J. 2001, *A&A*, 376, 85
 Kennicutt, R. C. 1983, *ApJ*, 272, 54
 —. 1989, *ApJ*, 344, 685
 —. 1998a, *ARA&A*, 36, 189
 —. 1998b, *ApJ*, 498, 541
 Khokhlov, A. M. 1998, *J.Comp.Phys.*, 143, 519
 Klypin, A., Kravtsov, A. V., Bullock, J. S., & Primack, J. R. 2001, *ApJ*, 554, 903
 Kravtsov, A. 2003, in preparation
 Kravtsov, A. V. 1999, PhD thesis, New Mexico State University
 Kravtsov, A. V., Klypin, A. A., & Khokhlov, A. M. 1997, *ApJS*, 111, 73
 Lin, D. N. C. & Pringle, J. E. 1987, *ApJ*, 320, L87
 Martin, C. L. & Kennicutt, R. C. 2001, *ApJ*, 555, 301
 Miller, G. E. & Scalo, J. M. 1979, *ApJS*, 41, 513
 Ostriker, E. C., Stone, J. M., & Gammie, C. F. 2001, *ApJ*, 546, 980
 Padoan, P., Nordlund, A., & Jones, B. J. T. 1997, *MNRAS*, 288, 145
 Schmidt, M. 1959, *ApJ*, 129, 243
 Silk, J. 2001, *MNRAS*, 324, 313
 Slyz, A. D., Devriendt, J. E. G., Silk, J., & Burkert, A. 2002, *MNRAS*, 333, 894
 Tassis, K., Abel, T., Bryan, G. L., & Norman, M. L. 2002, preprint [astro-ph/0212457](https://arxiv.org/abs/astro-ph/0212457)
 Vázquez-Semadeni, E., Gazol, A., & Scalo, J. 2000, *ApJ*, 540, 271
 van Leer, B. 1979, *J.Comp.Phys.*, 32, 101
 Vázquez-Semadeni, E. 1994, *ApJ*, 423, 681
 Wada, K. & Norman, C. A. 2001, *ApJ*, 547, 172
 Wong, T. & Blitz, L. 2002, *ApJ*, 569, 157
 Woosley, S. E. & Weaver, T. A. 1995, *ApJS*, 101, 181
 Young, J. S., Allen, L., Kenney, J. D. P., Lesser, A., & Rownd, B. 1996, *AJ*, 112, 1903